Macromolecular Research, Vol. 11, No. 6, pp 425-430 (2003)

Poly(*n*-butyl acrylate-*co*-methyl methacrylate) and Poly(*n*-butyl acrylate-*co*-styrene)/ Silicate Nanocomposites Prepared by Emulsion Polymerization

Yeong Suk Choi and In Jae Chung*

Department of Chemical and Biomolecular Engineering,Korea Advanced Institute of Science and Technology, 373-1, Guseong-dong, Yuseong-gu, Daejeon 305-701, Korea

Received Mar. 26, 2003; Revised Oct. 7, 2003

Abstract: Two types of poly(*n*-butyl acrylate) copolymer/silicate nanocomposites have been produced: poly(*n*-butyl acrylate-*co*-methyl methacrylate) [P(BA-*co*-MMA)]/silicate nanocomposites and poly(*n*-butyl acrylate-*co*-styrene) [P(BA-*co*-ST)]/silicate nanocomposites. The P(BA-*co*-MMA)/silicate nanocomposites shows the exfoliated structures but a P(BA-*co*-ST)/silicate nanocomposites have intercalated structures, because the BA/MMA comonomer has a higher polarity (e-value in Q-e scheme) than the BA/ST comonomer. The BA/MMA comonomer expanded the interlayer space of the silicate wider than did the BA/ST comonomer. The thermal degradation onset point of the P(BA-*co*-MMA)/silicate nanocomposites was 43 °C higher than that of pure P(BA-*co*-MMA). P(BA-*co*-MMA)T5%, P(BA-*co*-MMA)T10%, and P(BA-*co*-MMA)T20% exhibit 134, 302, and 195% increases, respectively, in their storage moduli at -20 °C relative to the pure copolymer.

Keywords: e-value, interaction, silicate, nanocomposite, basal spacing.

Introduction

Conventional organic/inorganic composites show good mechanical properties with optimum amount of inorganic fillers. It indicates that the mechanical properties of conventional composites depend on dispersion state of inorganic fillers in organic matrices, interfacial interaction between organic matrices and inorganic fillers, and size of fillers. These factors need to be considered for polymer/phyllosilicate (hereafter abbreviated as silicate) nanocomposites, because mechanical properties of the nanocomposites will be affected by dispersion state of silicate particles and individual layers. The main focus on production of polymer/silicate nanocomposites[1-8,22,23] is to obtain exfoliated state of silicate layers in polymer matrix, because exfoliated polymer/silicate nanocomposites have most high dispersion state of silicate that offers the enhanced mechanical properties. Hydrophilicity and narrow basal spacing of pristine silicate retard producing the exfoliated nanocomposites with hydrophobic polymers. So, modifiers such as alkyl ammoniums are introduced to change the hydrophilic silicates hydrophobic (organoclays) and enlarge basal spacings of silicates. Most alkyl ammoniums have low thermal and mechanical properties compared to polymer matrix in the nanocomposites, so the decrease in mechanical properties of the nanocomposites prepared with organoclays seems to be inevitable. Understanding the exfoliation mechanism of silicates will facilitate the synthesis of the exfoliated polymer/silicate nanocomposites using pristine silicates. Sodium montmorillonite (Na-MMT), one of phyllosilicates, composes of two tetrahedral silicone-oxide sheets and one octahedral aluminum-oxide sheet in a layer. Na-MMT can imbibe organic materials through various mechanisms:[24] cationic bondings (substituting sodium cations with alkyl ammoniums), ion-dipole interactions (sodium cations and polar molecules), dipole-dipole interactions (polar molecules and siliconeoxide), hydrogen bondings, and π-bondings. The interactions are mainly based on polarity of organic molecules except cationic bondings, and most vinyl monomers have an useful scale of polarity, e-value of Q-e scheme.[21] The interaction between pristine silicates and vinyl monomers will be explained simply with e-values of monomers and gap size of the silicates. Dispersion component (δ_d) in Hansen solubility parameters ($\delta_t^2 = \delta_d^2 + \delta_p^2 + \delta_h$)[25] become dominant for the dispersion state of organoclays in organic solvents,[26] but polar component (δ_p) and hydrogen component (δ_h) will not be neglected in dealing with pristine silicates. The polar component (δ_p) and the hydrogen component (δ_h) are related with dipoles or polarities of monomers, so two components can be transferred into e-values.

Poly(*n*-butyl acrylate) copolymers are chosen for the pur-

*e-mail: chung@kaist.ac.kr

pose, because they have wide applications such as toughners, shock-absorbers, adhesives for plastics or papers.[9-17] One polar monomer (methyl methacrylate) and one nonpolar monomer (styrene) are selected as comonomers for producing poly(*n*-butyl acrylate) copolymer/silicate nanocomposites, because they have different polarities. In this paper, the chemical affinities of BA, MMA, ST, mixtures of BA/MMA, and BA/ST with silicate layers will be examined in association with the basal spacings of silicate in monomer/silicate dispersion states and with the e-values of monomers. Structure of polymer/silicate nanocomposites prepared by a semi-batch emulsion polymerization will be examined using X-ray and TEM. Finally we will investigate thermal and mechanical properties of the nanocomposites with TGA, and DMA.

Experimental

Materials. *n*-butyl acrylate (BA), methyl methacrylate (MMA), styrene (ST), dodecylbenzenesulfonic aicd sodum salt (DBS-Na), and 2-acrylamido-2-methyl-1-propanesulfonic acid (AMPS)[18-20] were purchased from Aldrich and used as received. The silicate used in this paper was sodium montmorillonite (Na-MMT) of Kunipia-F purchased from Kunimine Co. and the silicate had 119 mequiv/100 g of cation exchange capacity. The pristine silicate was dispersed in deionized water for 12 hrs at an ambient temperature before polymerization. Potassium persulfate (KPS) of Junsei, a radical initiator, was recrystallized using deionized water. Tetrahydrofuran (THF) of HPLC solvent grade was used as received from Fluka for extraction. Methyl alcohol (MeOH) of Fluka, a nonsolvent for copolymers, was distilled at a normal pressure. Lithium chloride (LiCl, Junsei) was recrystallized with THF.

Synthesis of P(BA-*co*-MMA) and P(BA-*co*-ST)/Silicate Nanocomposites. Poly(*n*-butyl acrylate-*co*-methyl methacrylate) [P(BA-*co*-MMA)] and poly(*n*-butyl acrylate-*co*-styrene) [P(BA-*co*-ST)]/silicate nanocomposites were synthesized through a semi-batch emulsion polymerization method as described in our previous paper except following conditions.[6-8] The ratio of ingredients in initial stage was 5 g /0.3 g/120 g/4 g [comonomer/AMPS/water/initiator aqueous solution (1 wt%)], and 15 g of comonomer was charged at a rate of 0.2 cc/min in incremental stage. Two types of comonomers were prepared by mixing BA (50 g)/MMA (50 g) and BA (50 g)/ST (50 g) magnetically before polymerization. Polymerization temperature was controlled isothermally at 75 °C throughout entire procedure. 1 g of DBS-Na (10 wt% of aqueous solution) was added to P(BA-*co*-ST)/silicate nanocomposites after initial polymerization for further stabilization.

Polymer Recovery. Copolymers were recovered by a method described in our previous paper.[6-8]

Measurements. X-ray, GPC, TGA, DMA, and TEM measurements for final copolymer/silicate nanocomposites were carried out as descried in our previous paper.[6-8]

A sample for TEM was molded with epoxy, and sliced in 70 nm thickness with a cyro-ultramicrotome system, CRX, of Boeckeler at liquid nitrogen temperature.

X-ray diffraction patterns of monomer/silicate dispersions were obtained by using a Rigaku X-ray generator (CuKα with $\lambda = 0.15406$ nm) on a glass holder under a scanning rate of 2 °/min in 2θ range of 1.5-10 ° at a room temperature. Monomers were added to the pristine silicate with a ratio of monomer/silicate (30 g/ 3 g) to saturate its basal space. The monomer/silicate mixtures were stirred for 48 hrs at 200 rpm.

Results and Discussion

Expansion of basal spacing of silicate by monomer will be important for polymer/silicate nanocomposites prepared through in-situ polymerizations, since at least two polymerization sites will consume monomers competitively: 1) inside silicate including surface 2) outside silicate (reaction medium or bulk monomer). If the polymerization rate outside silicate particle is so fast to deplete most monomers, the polymerization rate inside silicate will decrease because polymerization rate is proportional to monomer concentrations. The degree of expansion of silicate basal spacing by monomer indicates the monomer concentration in the silicate galleries and affects the rate of polymerization. So the basal spacing of silicate before polymerization may predict the structure of polymer/silicate nanocomposites.

Figure 1 shows X-ray diffraction patterns of monomer/silicate dispersions. The basal spacing, d_{001}, of silicate layers at

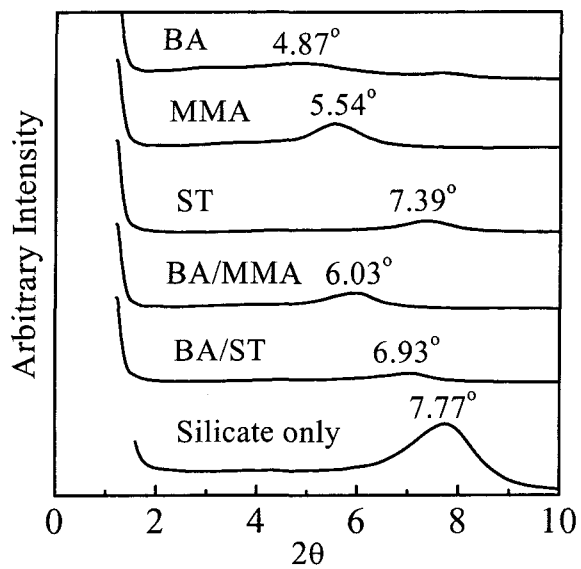

Figure 1. X-ray diffraction patterns of monomer/silicate mixtures dispersed with a ratio of monomer/silicate (30 g/3 g). Pristine silicate is given as a reference.

a peak position is calculated from the Bragg's law. The silicates saturated with BA, MMA, ST, and BA/MMA, BA/ST mixtures show peak shift from its dry state position to low angle positions. The silicate containing *n*-butyl acrylate (BA/silicate) shows the (001) plane diffraction peak at 4.87° in 2θ value and has the basal spacing of 1.81 nm. MMA/silicate shows the peak at 5.54° and the basal spacing of 1.60 nm. ST/silicate shows the peak at 7.39° and the basal spacing of 1.20 nm. BA/MMA/silicate shows the peak at 6.03° and the basal spacing of 1.47 nm. BA/ST/silicate shows the peak at 6.93° and the basal spacing of 1.27 nm. BA/MMA/silicate dispersion shows the narrower basal spacing than BA or MMA/silicate dispersions, and it may involve two competitive interactions: 1) interaction between silicate and mixed monomer 2) interaction between two polar monomers themselves. The interaction between two polar monomers seems to be dominant. BA, MMA,[25] ST[27] have similar total solubility parameters (Hildebrand solubility parameter) of 17.7(BA), 17.9 (MMA), 19.0 (ST) M/Pa$^{1/2}$, but the basal spacing of silicate with monomers are quite different. Furthermore ST monomer has the most high dispersion component value (δ_d), but expands the less basal spacing. BA and MMA have higher polar component (δ_p) and hydrogen component (δ_h) than those of ST as listed in Table I. It indicates that the polar component (δ_p) and the hydrogen component (δ_h) mainly affect the expansion of the basal spacings rather than the dispersion component (δ_d) for the pristine silicate. The two components (δ_p, δ_h) are based on polarities, so they can be combined into a polarity value scale, evalue in Q-e scheme.[21]

Figure 2 shows the evalues of monomers and the variation of basal spacings of silicate after monomer adsorption. The basal spacings of silicate dispersions appear in the following order: BA (0.85) > MMA (0.4) > BA/MMA (0.6) > BA/ST (-0.06) > ST (-0.6). The value in the parenthesis is e-value. The basal spacings of silicate by monomer adsorption follow the e-value of each monomer. These results explain that as the polarity of monomer become high, the basal spacings of the silicate increase, which means that the amounts of monomers in the space increase. In the expanded state, monomers and initiators in aqueous phase can easily penetrate into the interlayer spaces of pristine silicate, and lead a very favorable environment for the production of exfoliated

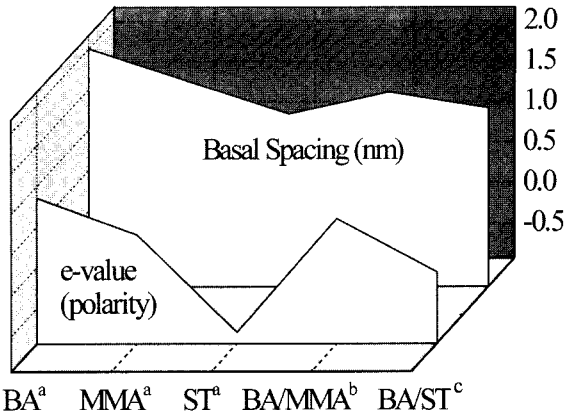

Figure 2. Plot of d_{001} spacing of silicate after adsorption of monomers and polarities of monomers.[a] Odian G. "Principles of Polymerization" 3rd ed. pp491.[21] [b]a value after calculation of molar concentration of BA and MMA and their evalues.[c]a value after calculation of molar concentration of BA and ST and their values.

copolymer/silicate nanocomposites.

Figure 3(a) shows almost no peak in X-ray diffraction patterns of P(BA-*co*-MMA)/silicate nanocomposites. Within 20 wt% of silicate loading, the nanocomposites are in exfoliated states. On the other hand, Figure 3(b) shows diffraction peaks at 4.90° (2.00 nm) in P(BA-*co*-ST)/silicate nanocomposite with 10 wt% of silicate and at 3.64° (2.70 nm) with 5 wt%, respectively. The X-ray diffraction patterns illustrate that the basal spacing of silicate adsorbed with monomers affects the dispersion states of silicate in polymer/silicate nanocomposites, and the expansion is affected very much by the e-values (polarities) of monomers.

Molecular weights of copolymers recovered from the nanocomposites are listed in Table I. The weightaverage molecular weight (M_w) of P(BA-*co*-MMA) decreases as the content of silicate in the nanocomposite increases. On the other hand, the number-average molecular weight (M_n) increases until 10 wt% of silicate but is low at 20 wt% of silicate loading. X-ray diffraction pattern of initiator/silicate aqueous dispersion is not given for simplicity, but the initiator penetrates into the basal spacing of silicate in aqueous dispersion. Under this condition, the variation in molecular weights of polymers from the nanocomposites may be inter-

Table I. Solubility Parameters of Monomers and Peak Positions of Monomer/Silicate Mixtures Obtained from X-ray Diffraction Patterns

Monomers	δ_d M/Pa$^{1/2}$	δ_p M/Pa$^{1/2}$	δ_h M/Pa$^{1/2}$	δ_t^a M/Pa$^{1/2}$	H-bonding Group	Peak Position(2θ)
n-butyl acrylate (BA)[25]	14.0	8.3	6.8	17.7	m	4.87°
Methyl methacrylate (MMA)[25]	13.7	9.8	6.1	17.9	m	5.54°
Styrene (ST)[27]	18.6	1.0	4.1	19.0	p	7.39°

[a] $\delta_t^2 = \delta_{td}^2 + \delta_{tp}^2 + \delta_{th}^2$ where δ_t is total solubility parameter that is equal to Hildebrand solubility parameter, δ_d is disperse component, δ_p is polar component, δ_h is hydrogen bonding component of Hansen solubility parameters.

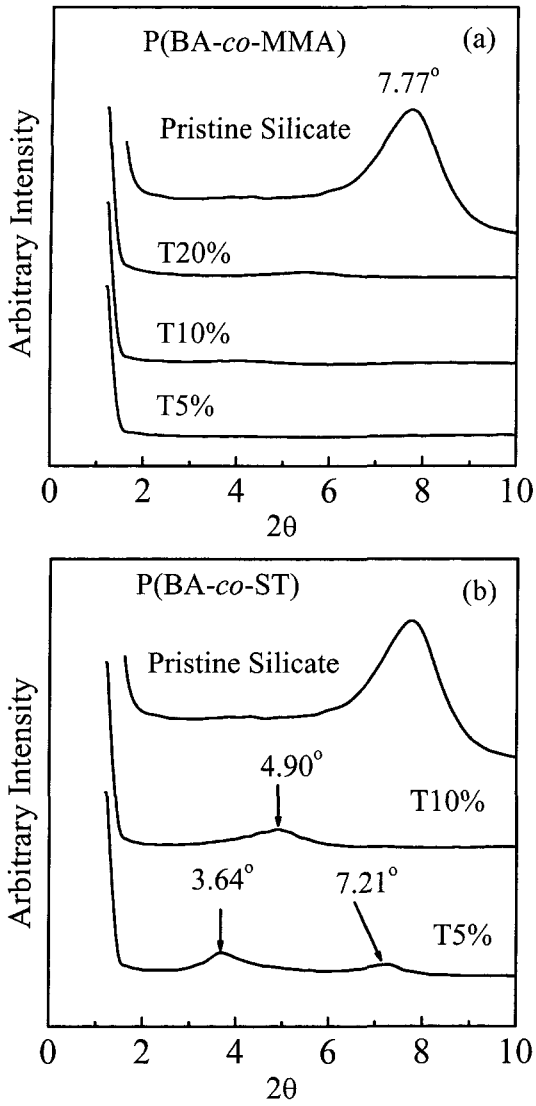

Figure 3. X-ray diffraction patterns of (a) P(BA-*co*-MMA)/silicate nanocomposites and (b) P(BA-*co*-ST)/silicate nanocomposites. Pristine silicate is given as a reference.

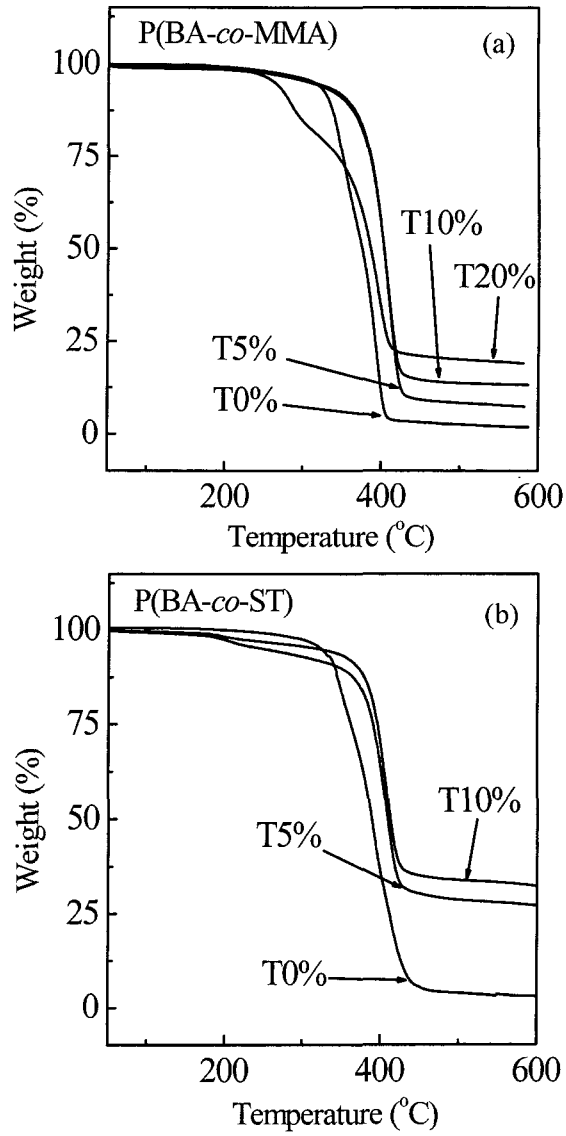

Figure 4. Thermal gravimetric curves for (a) P(BA-*co*-MMA)/silicate nanocomposites and (b) P(BA-*co*-ST)/silicate nanocomposites. T#% indicates the weight percentage of pristine silicate added to monomer.

preted as follows: since silicate absorbs monomers, initiators, and AMPS in the interlayer space of silicate, polymerization occurs inside the silicate particles. As the amount of silicate increases, the relative amount of monomer will decrease, and the molecular weight of polymers will decrease. On the other hand, P(BA-*co*-ST) series show little changed as the content of silicate increases, and it seems to involve in the low yields of the nanocomposites.

Figure 4 shows thermogravimetric analyses (TGA) as a function of weight losses of nanocomposites and the pure copolymer. Onset point due to thermal decomposition shifts toward a higher temperature as the amount of pristine silicate increases except P(BA-*co*-MMA)T20%. The onset points of P(BA-*co*-MMA)T5% and P(BA-*co*-MMA)T10% appear at 358 °C, showing 43 °C higher temperature than pure P(BA-*co*-MMA), while P(BA-*co*-MMA)T20% shows the onset point at 242 °C, because, we think, the low molecular weight of the copolymer in the nanocomposite brings down the thermal stability (refer to Table II). The main chains of P(BA-*co*-MMA) decompose thermally in the temperature range of 358-450 °C. The onset points of P(BA-*co*-ST)T5% and P(BA-*co*-ST)T10% occur at 374 °C but their residual amounts at 600°C are 27.2 and 32.4% indicating the low yield of polymerization. The TGA curves explain that the thermal properties of polymer/silicate nanocomposites will be influenced by the amounts of silicate loading and the molecular weights of polymers matrix. On the other hand, the yields of P(BA-*co*-ST) series may be related to the diffu-

Table II. Molecular Weights of Poly(*n*-butyl acrylate) Copolymers Recovered from Copolymer/Silicate Nanocomposites

Codes for Nanocomposites	M_n	M_w	PDI (M_w/M_n)	Yield (%)
P(BA-*co*-MMA)T0%	284,900	1,410,700	4.95	100
P(BA-*co*-MMA)T5%	284,800	1,202,700	4.22	92.1
P(BA-*co*-MMA)T10%	350,200	1,056,300	3.01	89
P(BA-*co*-MMA)T20%	130,100	765,000	5.88	100
P(BA-*co*-ST)T0%	102,100	3357,350	3.50	100
P(BA-*co*-ST)T5%	85,300	307,400	3.60	21.1
P(BA-*co*-ST)T10%	99,500	312,100	3.13	34.2

sion in chain growth,[28] since hydrophobic styrene will experience difficulty to diffuse into silicate particles by the hydrophilicity of silicate layers.

The yields of P(BA-*co*-ST)/silicate nanocomposites were too low for measurement of mechanical property, so P(BA-*co*-MMA)/silicate nanocomposites were subjected to measure DMA. The storage moduli, E', of P(BA-*co*-MMA) series at -20 °C increase with the amount of pristine silicate as shown in Figure 5. The pure P(BA-*co*-MMA) has the storage modulus of 6.36×10^8 Pa. P(BA-*co*-MMA)T5%, P(BA-*co*-MMA)T10%, and P(BA-*co*-MMA)T20% have 1.49×10^9 Pa, 2.56×10^9 Pa, and 1.88×10^9 Pa, showing 134%, 302%, and 195% increase when compared to the pure copolymer. P(BA-*co*-MMA)T20% has the higher content of silicate but the lower storage modulus than P(BA-*co*-MMA) T10%, because the former has the lower molecular weight of copolymer than the latter. The moduli of the nanocomposites explain that the enhancement may relate to the amount of silicate loading and the molecular weight of polymer matrix.

Distribution degree of silicate layers in the polymer matrix will affect glass transition temperatures (T_g) of the nanocomposites. Glass transition temperature (T_g) of P(BA-*co*-MMA)/silicate nanocomposite is obtained with the maximum value in the temperature versus tan δ plot in Figure 6. The glass transition temperatures (T_g) are 40.9 °C for pure copolymer, 44.8 °C for P(BA-*co*-MMA)T5%, 37.8 °C for P(BA-*co*-MMA)T10%, and 41.2 °C for P(BA-*co*-MMA)T 20%. The glass transition temperatures (T_g) of P(BA-*co*-MMA)/silicate nanocomposites slightly shift toward higher temperatures. The values of tan $\delta(=E''/E')$ for the nanocomposites become low as the content of silicate loading increases, which reflects the high fluidity of the nanocomposites.

Figure 7 shows the TEM image of P(BA-*co*-MMA)T5%. Individual silicate layers are dispersed uniformly in copolymer matrix, and it reconfirms the exfoliation of silicate layers in the nanocomposite.

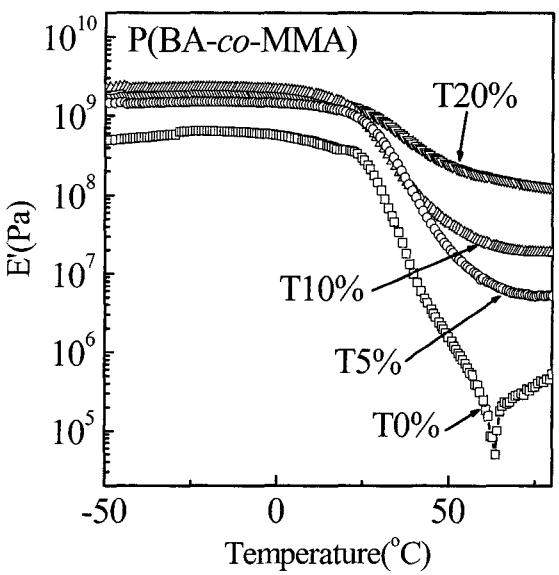

Figure 5. Dependence of storage modulus of P(BA-*co*-MMA)/silicate nanocomposites and the pure copolymer.

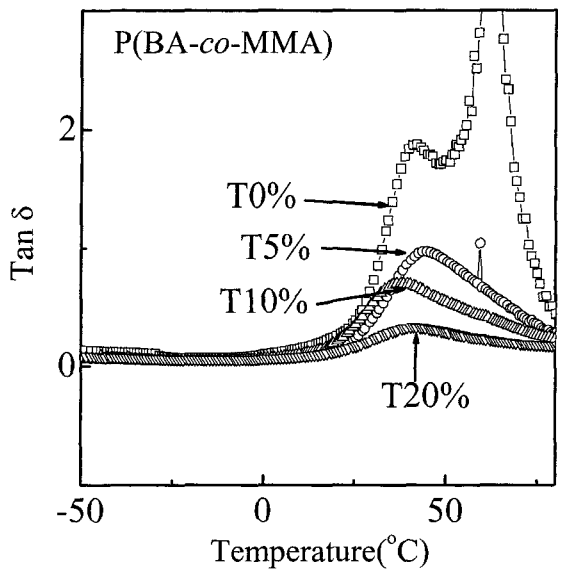

Figure 6. Tan δ of P(BA-*co*-MMA)/silicate nanocomposites and the pure copolymer.

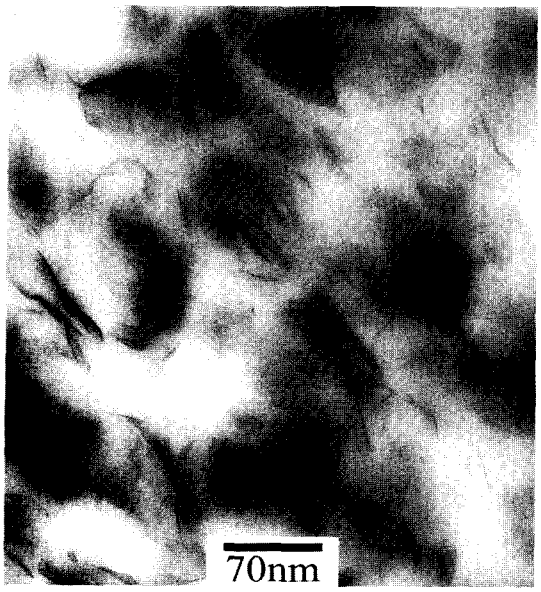

Figure 7. TEM micrographs of P(BA-*co*-MMA)/silicate nanocomposite containing 5 wt % of silicate.

Conclusions

In this paper, we report exfoliated P(BA-*co*-MMA)/silicate nanocomposites for the first time. Pristine silicate saturated with BA, MMA, ST, BA/MMA comonomer (50 g/50 g), and BA/ST comonomer (50 g/50 g) show different basal spacings according to monomer polarities: BA (e-value: 0.85) > MMA (0.4) > BA/MMA (0.6) > BA/ST (-0.06) > ST (-0.6). The peaks in X-ray diffraction patterns appear at 4.87° for BA/silicate, at 5.54° for MMA/silicate, at 7.39° for ST/silicate, at 6.03° for BA/MMA/silicate, and at 6.93° for BA/ST/silicate. It indicates that the monomer with high polarity makes the basal spacing of silicate wide, and the degree of expansion of silicate layer space by monomers affects the resultant morphology of copolymer/silicate nanocomposite showing exfoliated structures for P(BA-*co*-MMA) series and intercalated structures for P(BA-*co*-ST) series. P(BA-*co*-MMA)/silicate nanocomposites showed improved properties in TGA and DMA anaylsis. P(BA-*co*-MMA)T5% and P(BA-*co*-MMA)T10% showed the 43 °C higher onset temperature of thermal decomposition than pure P(BA-*co*-MMA) in thermogravimetric analyses (TGA). The storage moduli of P(BA-*co*-MMA)T5%, P(BA-*co*-MMA)T10%, and P(BA-*co*-MMA)T20% are 1.49×10^9 Pa, 2.56×10^9 Pa, and 1.88×10^9 Pa showing 134%, 302%, and 195% enhanced compared to that of the pure copolymer.

Acknowledgements. Authors thank KOSEF (Korea Science and Engineering Foundation), CAFPoly (Center for Advanced Functional Polymers), and BK 21 program for their financial support.

References

(1) G. D. Kim, D. H. Lee, B. Hoffmann, J. Kressler, and G. Stöppelmann, *Polymer*, **42**, 1095 (2001).
(2) M. W. Noh and D. C. Lee, *Polym. Bull.*, **42**, 619 (1999).
(3) M. Okamoto, S. Morita, H. Taguchi, Y. H. Kim, T. Kotaka, and H. Tateyama, *Polymer*, **41**, 3887 (2000).
(4) B. Hoffmann, C. Dietrich, R. Thomann, C. Friedrich, and R. Mülhaupt, *Macromol. Rapid Commun.*, **21**, 57 (2000).
(5) H. Y. Byun, M. H. Choi, and I. J. Chung, *Chem. Mater.*, **13**, 4221 (2001).
(6) Y. S. Choi, M. H. Choi, K. H. Wang, S. O. Kim, Y. K. Kim, and I. J. Chung, *Macromolecules*, **34**, 8978 (2001).
(7) Y. S. Choi, K. H. Wang, M. Xu, and I. J. Chung, *Chem. Mater.*, **14**, 2936 (2002).
(8) Y. K. Kim, Y. S. Choi, K. H. Wang, and I. J. Chung, *Chem. Mater.*, **14**, 4990 (2002).
(9) M. Schneider, T. Pith, and M. Lambla. *Polym. Adv. Technol.*, **7**, 425 (1996).
(10) I. Luzinov, A. Voronov, S. Minko, R. Kraus, W. Wilke, and A. Zhuk, *J. Appl. Polym. Sci.*, **61**, 1101 (1996).
(11) M. W. C. Wahls and J. C. Leyte, *Appl. Spectrosc.*, **52**, 123, (1998).
(12) F. Ziaee and M. Nekoomanesh, *Polymer*, **39**, 203 (1998).
(13) A. S. Brar and S. Charan, *J. Polym. Sci., Part A: Polym. Chem.*, **33**, 109 (1995).
(14) K. Yamada, T. Nakano, and Y. Okamoto, *Polym. Sci., Part A: Polym. Chem.*, **38**, 220 (2000).
(15) H. A. S. Schoonbrood, M. J. Unzué, O. Beck, and J. M. Asua, *Macromolecules*, **30**, 6024 (1997).
(16) P. Hazot, C. Pichot, and A. Maazouz, *Macromol. Chem. Phys.*, **201**, 632 (2000).
(17) H. Ni, G. Ma, M. Nagai, and S. Omi, *J. Appl. Polym. Sci.*, **76**. 1731 (2000).
(18) M. Seki, Y. Morishima, and M. Kamachi, *Macromolecules*, **25**, 6540 (1992).
(19) Y. Morishima, S. Nomura, T. Ikeda, M. Seki, and M. Kamachi, *Macromolecules*, **28**, 2874 (1995).
(20) H. Aota, S. I. Akaki, Y. Morishima, and M. Kamachi, *Macromolecules*, **30**, 4090 (1997).
(21) G. Odian, *Principles of Polymerization*, 3rd ed., Wiley, New York, 1991.
(22) J. G. Ryu, J. W. Lee, and H. Kim, *Macromol. Res.*, **10**, 187 (2002).
(23) N. G. Sahoo, C. K. Das, A. B. Panda, and P. Pramanik, *Macromol. Res.*, **10**, 369 (2002).
(24) R. F. Giese and C. van Oss, *J. Colloid and Surface Properties of Clays and Related Minerals*, Marcel Dekker Inc., New York, 2002.
(25) A. F. M. Barton, *CRC Handbook of Solubility Parameters and Other Cohesion Parameters*, CRC Press, Boca Raton, 1991.
(26) D. L. Ho and C. J. Glinka, *Chem. Mater.*, **15**, 1309 (2003).
(27) J. Brandrup and E. H. Immergut, *Polymer Handbook*, 4th ed., Wiely, New York, 1999.
(28) F. Ziaee and M. Nekoomanesh, *Polymer*, **39**, 203 (1998).